Hindawi
Shock and Vibration
Volume 2019, Article ID 1232350, 13 pages
https://doi.org/10.1155/2019/1232350

Research Article

Performance Analysis of Piezoelectric Actuators in Railway Wheel Squealing Noise Mitigation

Seyed Rahim Marjani and Davood Younesian

Center of Excellence in Railway Transportation, School of Railway Engineering, Iran University of Science and Technology, Tehran 16846-13114, Iran

Correspondence should be addressed to Davood Younesian; younesian@iust.ac.ir

Received 18 June 2019; Revised 9 August 2019; Accepted 1 October 2019; Published 23 October 2019

Academic Editor: Chengzhi Shi

Application of a shunted piezoelectric system in reduction of the squeal noise level in railway wheels is studied. A wheel squeal model including the railway track, wheel, and nonlinear interaction contact forces is taken into account in the time domain. Consequent vibration of the wheel is calculated at incident of sharp curve passing. The sound pressure level (SPL) of the noise is then calculated by an analytical method. Performance of different shunt circuits including the *R* (resistance) and *RL* (resistance inductance) is evaluated in different frequency ranges. A new methodology is proposed to achieve multimode damping. According to results, the SPL of wheel squeal noise can effectively get reduced by the proposed method, up to 5 dB at near-field and 10 dB at far-field.

1. Introduction

The monotonic, disturbing, and high-level noise is often addressed as squealing noise. This unpleasant noise can be generated during the passage of railcar through sharp curves and/or during braking of railway vehicles. Occurrence of the squealing noise has been reported not only for passenger trains but also for metro and tram lines. This annoying noise is a normal consequence of the stick-slip phenomenon depending on both wheel and rail modal characteristics and contact patch reactive forces. Several major problems can be caused by the squealing noise due to the fact that the radiated noise not only affects the comfort of train passengers, but it can also disturb residents of nearby buildings [1, 2]. In urban regions, railway noise can even become a more important problem due to presence of buildings so that high-level railway noise remarkably increases environmental costs. Wear and tear has also been reported both in wheel and rail due to such a stick-slip harsh motion.

Numerous experimental and analytical studies have been conducted in recent years to understand the wheel squeal noise, to predict its sources, and to investigate potential methods for mitigation of that problem. For this purpose, experimental field measurements have been carried out by a number of researchers [3–7]. Obtained results of these experimental investigations show that the wheel squeal occurs in inner wheels and axial vibrating modes of the wheel are the main source of the noise. Furthermore, different test rigs have been designed to investigate effects of different parameters on the squealing in laboratory scales [8–10]. These studies indicate that the negative slope of the friction coefficient-creepage curve during the large creepage plays an important role in generation of the wheel squeal. According to the laboratory and field experimental measurements, increasing wheel damping is a very effective solution for wheel squeal suppression. In some other research projects, different analytical wheel squeal models have been developed and validated employing test results. A comprehensive model including the track, wheel, nonlinear contact forces, and rail vehicle was provided by Thompson and Monk-steel [11]. This model was used to investigate the influence of rail and wheel contact position on the occurrence of the squeal noise. Supplementary analytical models in the time domain can also be found in [11–16], applied for

studying various aspects of the wheel squeal noise. Most recently, a number of scientists have tried to introduce simplified and practical models. Examples of such studies can be found in [17, 18]. Liu and Meehan [17] presented a simplified model using an energy-based approach to study influence of the velocity and angle of attack. A simplified contact theory was applied by Zenzerovic et al. [18] in order to presenting an engineering model for the wheel squeal. Younesian et al. [19] proposed an analytical method and obtained the noise radiated from a vibrating wheel.

Although prediction of the squealing noise is a significant task for researchers, proposing a suitable method for mitigation of this noise is necessary. Therefore, in addition to the research studies conducted on the squealing measurement, modeling and its calibrating, and various methods for mitigation of the wheel squeal noise have also been reported. Muller and Oertli [20] proposed a solution strategy based on the friction modification and asymmetric grinding. They examined the effectiveness of their idea by performing a number of measurements. Rail lubrication was proposed and studied by different authors [21–23]. It was found that this method can help to reduce the noise level. However, the method has some disadvantages as well since it results in a higher maintenance cost and may increase the rail/wheel loss of adhesion. Hiensch and Lammers [24] proposed railhead shape optimization to avoid railway squeal noise. Increasing wheel damping is a verified method for suppression of the wheel squeal, and its efficiency has analytically and experimentally been proven. In order to enhance wheel damping, diverse methods have been proposed so far. We may address to (a) preloaded rings inserted into the wheel [25], (b) mounting damping layers to the wheel [4, 26] and carbody [27], and (c) dynamic vibration absorbers [28]. Each method has its own costs and benefits. Performance of the inserted rings in the wheel was shown to be not precisely predictable. Damping layers cannot optimally act in narrow-band frequencies. Design procedure of the efficient dynamic vibration absorbers is complex, and their reaction time responses are normally high. This study is intended to present a new creative solution based on the shunted piezoelectric elements. These elements have widely been employed for vibration absorption, both in laboratory applications and industry full-scales. A comprehensive survey of the application of piezoelectric transducers and shunt circuits has been presented by Moheimani and Fleming [29]. Vibration control of a flexible spacecraft [30], wind turbine blade [31], and railway vehicle carbody [32] are some of successful experiences of the shunted piezoelectric applications. Jakob et al. [33] experimentally investigated active vibration control of rail wheels by using piezoelectric actuators. In a very recent study, Marjani and Younesian [34] employed the Nyquist method and investigated the performance of piezoelectric elements in postponing and reducing probability of the wheel sequel in the frequency domain. Followed to the previous study, in this paper, the authors evaluate application of shunted piezoelectric in squeal noise level reduction. The two main open questions to be answered here are as follows: (a) How efficient would the piezoelectric elements act in the real-time domain? How much of the wheel squeal sound pressure level (SPL in dB) can be reduced by this system? (b) Are they capable of performing multimode reductions? In order to answer these open questions, application of shunted piezoelectric for reduction of wheel squeal noise is studied in this paper. First, the wheel squeal is comprehensively modeled in the time domain. The model includes railway track, wheel, and nonlinear interaction contact forces. Sound pressure level (SPL) of the noise is then calculated. In the next step, shunted piezoelectric elements are attached to the wheel, and their effects on the wheel dynamic characteristics are taken into account. Performance of different shunt circuits including the R and RL is investigated at different desired frequencies. Also multimode damping is achieved by dividing piezoelectric patches into two groups with different shunt circuits. According to the obtained results, the SPL of wheel squeal noise can significantly be reduced by using adequate piezoelectric elements with adjusted shunt circuit parameters. Shunted piezoelectric can produce damping more than 2% in axial modes, which is noticeably more than other reduction methods.

2. Transient Wheel Squeal Model

A model is developed in this section in order to predict railway wheel squeal. Different parts of the model including wheelset, railway track, and nonlinear wheel/rail contact are discussed in this section. The wheel and rail time-domain responses are then obtained and employed to calculate the radiated sound in sound pressure level (SPL).

2.1. Wheelset Dynamics. High-frequency vibration of railway wheel has been proven to be the main source of the wheel squeal [7]. Therefore, a precise and reliable wheelset dynamic model is necessary for the prediction of squeal noise. In the first part of this study, natural frequencies and mode shapes of the wheelset in desired frequency range are obtained by using a finite element (FE) model. Damping for each mode is assumed as follows [35]:

$$\eta = \begin{cases} 0.001, & n = 0, \\ 0.01, & n = 1, \\ 0.0001, & n \geq 2, \end{cases} \tag{1}$$

where n is nodal circle. The wheelset dynamic characteristic equations are considered in the state-space domain as follows [28]:

$$\dot{\overline{\mathbf{y}}}^{w} = [\mathbf{A}^{w}]\overline{\mathbf{y}}^{w} + [\mathbf{B}^{w}]\overline{f}^{w}, \overline{v}^{w} = [\mathbf{C}^{w}]\overline{\mathbf{y}}^{w}. \tag{2}$$

In the above equations, $\overline{\mathbf{y}}_{w}$ denotes a $2n$-order state-variable vector including modal velocity $\dot{\overline{q}}_{r}$ and the modal displacement $\overline{q}_{r}$ of the modes r ($r = 1$ to n):

$$\overline{\mathbf{y}}^{w} = \{\dot{q}_1, \dot{q}_2, \ldots, \dot{q}_n, q_1, q_2, \ldots, q_n\}^{T} = \{y_1^{w}, y_2^{w}, \ldots, y_{2n}^{w}\}^{T}. \tag{3}$$

Moreover, n is the number of considered modes and $\overline{f}^{w} = \{f_2^{w}, f_3^{w}\}$ and $\overline{v}^{w} = \{v_2^{w}, v_3^{w}\}$ denote the input dynamic forces and output dynamic velocities in lateral and vertical

direction, respectively. The system matrix $[\mathbf{A}^w]$, the input matrix $[\mathbf{B}^w]$, and output matrix $[\mathbf{C}^w]$ can be obtained using the modal data in the state space.

2.2. Track Dynamics. The rail vibration does not directly contribute to the wheel squeal noise; however, the track dynamics influence the wheel/rail contact forces. The track dynamic is modeled in both vertical and lateral directions. As shown in Figure 1, the rail is assumed to be modeled by three attached beams [36]. Two infinite Timoshenko beams are used for the railhead and foot modeling, connected by using the third beam known as the rail web.

Sleepers are considered as concentrated mass elements, and vertical, lateral, and torsional stiffness of the rail pads and ballast are modeled by utilizing separate linear springs and dashpots in series, as shown in Figure 2.

Frequency response of the track is calculated by employing appropriate commercial FEM package, in both vertical and lateral directions. The equations of motion of the track in the state space are then provided by using the similar method employed for the wheel dynamics:

$$\dot{\overline{y}}^r_{2,3} = \left[A^r_{2,3}\right]\overline{y}^r_{2,3} + \left[B^r_{2,3}\right]\overline{f}^r_{2,3}, \tag{4}$$

$$\overline{v}^r_{2,3} = \left[C^r_{2,3}\right]\overline{y}^r_{2,3}. \tag{5}$$

2.3. Contact Theory. The wheel and rail contact coordinate system 1-2-3 is shown in Figure 3.

Because of the creepage in contact patch, the train speed does not precisely correspond to the wheel speed. Relation between lateral force F_2 and lateral creepage γ_2 can be represented by

$$F_2 = \mu_2(\gamma_2)F_3. \tag{6}$$

Lateral friction coefficient μ_2 can be calculated here, and F_3 is vertical force. Lateral friction coefficient can be obtained as follows [13]:

$$\mu_2 = \begin{Bmatrix} \mu_0\left(\Gamma_2 - \frac{1}{3}\Gamma_2^2 + \frac{1}{27}\Gamma_2^3\right), & \text{for } \Gamma_2 < 3, \\ \mu_0, & \text{for } \Gamma_2 > 3 \end{Bmatrix}, \tag{7}$$

where μ_0 denotes the rolling friction coefficient [13],

$$\mu_0(\gamma_2) = \mu_{\text{stat}}\left\{1 - 0.5e^{-0.138/|\gamma_2 V|} - 0.5e^{-6.9/|\gamma_2 V|}\right\},$$
$$\mu_{\text{stat}} = \frac{\tau_R \tau_W}{\tau_R + \tau_W}\frac{\pi ab}{N}. \tag{8}$$

In the latter equations, V is the train speed, τ_W, τ_R are the shear strength of the wheel and rail material (N/m^2), a and b are the semiaxis length of the Hertz contact ellipse in the rolling and lateral direction (m), and N is the static vertical force on the contact patch. In equation (7), Γ_2 is the normalized creepage given as

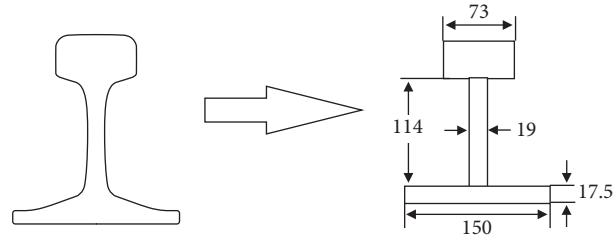

Figure 1: Modeling of the UIC 60 rail cross section (dimension are given in mm) [36].

$$\Gamma_2 = \frac{GC_{22}ab}{\mu_0 N}\gamma_2, \tag{9}$$

where G is the shear modulus of steel and C_{22} is the Kalkar constant presented in [37]. Moreover, F_3 is the vertical force in contact point which can be found as follows [13]:

$$F_3 = N + k_h \cdot \Delta y_3,$$
$$\Delta y_3 = \left(y_3^w - y_3^r\right), \tag{10}$$

where k_h is the Hertzian contact spring stiffness and y_3^w and y_3^r denote the wheel and rail vertical deflections at the contact point, respectively.

2.4. Transient Wheel Squeal Model. In order to model the wheel squeal in the time domain, dynamics of the wheel, rail, and contact forces are combined in a loop, as shown in Figure 4. First, a disturbance is exerted into the system to obtain the wheel and rail dynamic responses. The wheel and rail dynamic responses are calculated by solving equations (1) and (2) for the wheel and equations (4) and (5) for the rail. They are applied for obtaining the lateral sliding and vertical deflection at the contact point. The consequent contact forces are then obtained using the contact theory provided in Section 2.3. The transient simulation can be carried out by the step-by-step integration.

2.5. Noise Calculation. The acoustic pressure in desired point P in a spherical coordinate can be obtained by employing the Rayleigh integral [28]:

$$p(R, \varphi, \phi, t) = \frac{\rho_0}{2\pi}\int_{A_{\text{wheel}}} \frac{1}{R}\ddot{y}_2^w\left(r, \theta, t - \frac{R}{c_0}\right)\mathrm{d}A, \tag{11}$$

where R is the distance of P to the source, c_0 and ρ_0 are the sound speed and air density, respectively, and $\ddot{y}_2^w$ is the wheel lateral acceleration. Time delay in equation (11) is used to take the arrival time from the source into account. The outside wheel surface is divided into surface elements, and the integral is calculated over the wheel surface. Then, by placement calculated p in the following equation the SPL can be obtained:

$$\text{SPL} = 20\log_{10}\left(\frac{p}{p_0}\right)\mathrm{d}b, \tag{12}$$

where p_0 is the reference sound pressure equal to 20 μPa.

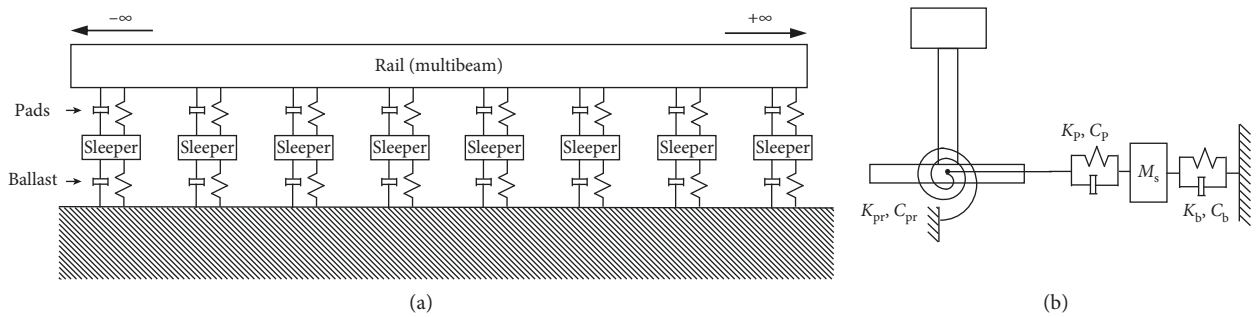

Figure 2: Railway track modeling [36]. (a) Top view. (b) Front view.

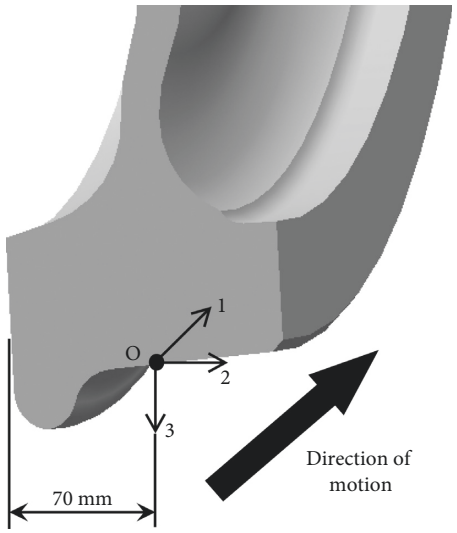

Figure 3: Coordinate system on the right wheel.

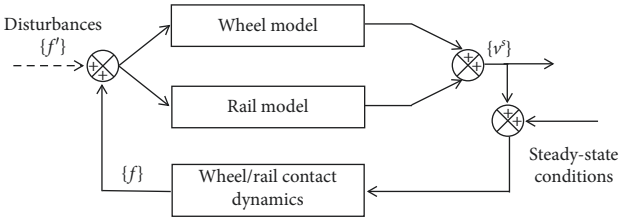

Figure 4: Loop of the wheel squeal transient modeling [13].

2.6. Shunted Piezoelectric. Application of shunted piezoelectric elements as structural dampers has been well addressed in recent decades. Piezoelectric patches convert the mechanical strain into electrical energy. By dissipating electrical energy in a shunt circuit, it can work as a virtual damper (Figure 5). Maximum damping in a desired frequency can be achieved by selecting adequate piezoelectric elements with adjusted position and tuned parameters. The location of maximum deformation in any mode shape must be considered to obtain maximum resultant electrical energy. Two types of the shunt circuits, *R* (resistor) and *RL* (resistor-inductor) circuits, are considered. The optimal values of the electrical parameters are obtained for each case. They can be adjusted to get the optimal performance in a specific frequency. Multimode damping can be achieved by attaching a group of piezoelectric patches in designated places. The procedure will be presented as a case study in the next section.

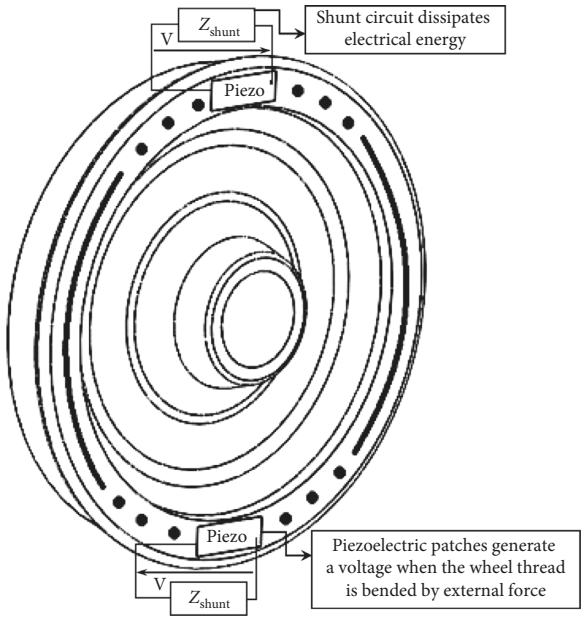

Figure 5: Shunted piezoelectric patches on the wheel thread.

2.6.1. Optimization of the Shunt Circuit. The purpose of optimization of shunt circuit is achieving maximum damping around specified frequencies. First, optimized parameters for *R* and *RL* circuits are approximated by the method presented by Hagood and Flotow [38]. The mechanical system with shunted piezoelectric around modal frequencies is modeled as the 1-DOF system, and an equivalent impedance is calculated as combination of the mechanical and electrical impedance for both types of shunt circuits (Figure 6).

Then, the equivalent impedance to get optimum parameters for *R* circuit is given by [38]

$$R_{\text{opt}} = \frac{\sqrt{1 - k_{31}^2}}{C_{\text{pi}}^S (2\pi\omega_t)}, \tag{13}$$

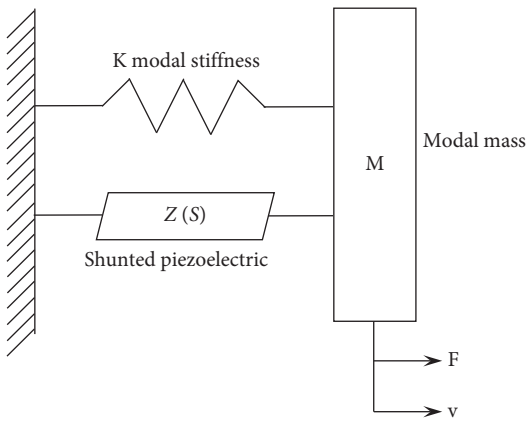

Figure 6: 1-DOF model of a system mode with shunted piezoelectric [38].

and for *RL* circuit by

$$R^{\text{opt}} = \frac{r^{\text{opt}}}{C_{\text{pi}}^2 \cdot \omega_n^E},$$
$$L^{\text{opt}} = \frac{C_{\text{pi}}^S}{\left(\delta^{\text{opt}} \cdot \omega_n\right)^2}, \tag{14}$$

where δ_{opt} and r_{opt} are optimized tuning parameter and damping parameter and can be calculated as follows:

$$\delta_{\text{opt}} = 1 + K_{ij}^2,$$
$$r_{\text{opt}} = 2\sqrt{\frac{K_{ij}^2}{\left(1 + K_{ij}^2\right)^3}}, \tag{15}$$

where K_{ij} is the generalized coupling coefficient and can be obtained by the following equation:

$$K_{ij}^2 = \frac{\left(\omega_n^D\right)^2 - \left(\omega_n^E\right)^2}{\left(\omega_n^E\right)^2}, \tag{16}$$

where ω_n^D and ω_n^E are open circuit natural frequency and short circuit natural frequency, respectively. These values are calculated by frequency analysis of the attached shunted piezoelectric wheel using the FEA software. Optimum parameters and corresponding harmonic response of the damped wheel around specified frequency is obtained by FEA software. A sample result is shown in Figure 7 for *RL* shunt circuits.

Corresponding added damping around specified frequency is calculated by the following equation:

$$\eta = \frac{\omega_2 - \omega_1}{2\omega_n}, \tag{17}$$

where ω_1, ω_2, and ω_n are presented in Figure 8.

3. Case Study

In this study, a bogie moving with a speed of 12.25 m/s through a curve of radius 300 is considered for finding the steady state curving parameters including the normal force, stationary lateral creepage, contact position, and stationary lateral friction coefficient and its slop. These parameters are listed in Table 1.

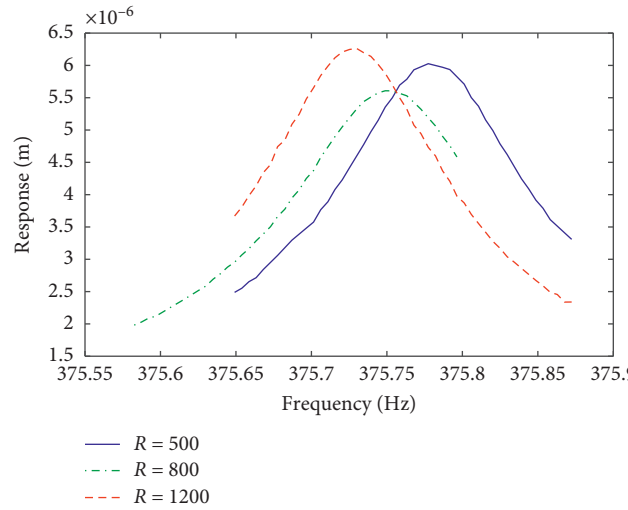

Figure 7: A sample of harmonic responses of damped wheelset.

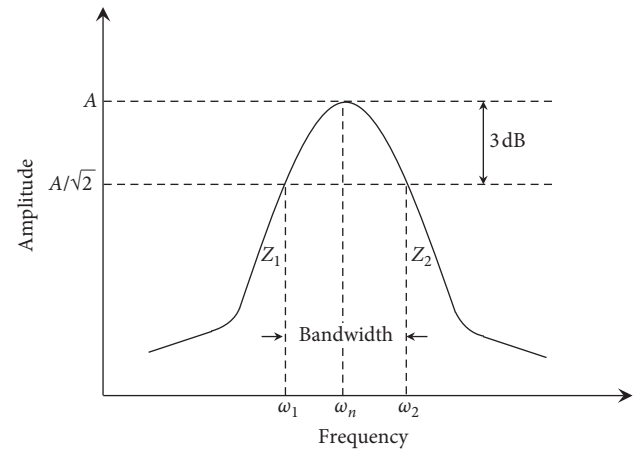

Figure 8: Calculation of damping.

A UIC920 wheelset with properties listed in Table 2 is taken into consideration. Obtained results from a FEA model including the natural frequencies and mode shapes are almost identical with the experimental results presented in [10]. The mode shapes of the wheel are similar to those of a circular thick plate. The main axial modes are shown in Figure 9. The axial modes are named (m, *n*), that *m* is nodal diameter and *n* is nodal circle. The axial modes with $n = 1$ have ten times larger damping (equation (1)) and practically do not appear in responses. Also modal frequencies of the modes with $n > 2$ are normally much higher than the frequency of squeal noise.

These modes have maximum lateral deformation and minimum damping. Hence they are the potential modes

Table 1: Steady state curving parameters [13].

Parameter	Symbol	Unit	Value
Normal force	N	kN	42
Stationary lateral creepage	γ_2	—	5.91×10^{-3}
Contact position	x_c	mm	13.4
Stationary lateral friction coefficient	μ_{stat}	—	0.398
Stationary lateral friction coefficient slope	$d\mu_2/d\lambda_2$	—	11.7

Table 2: Wheel material properties [13].

Parameter	Symbol	Unit	Value
Elastic modulus	E	GPa	200
Density	ρ	kg/m^3	7850
Poisson's ratio	ν	—	0.3

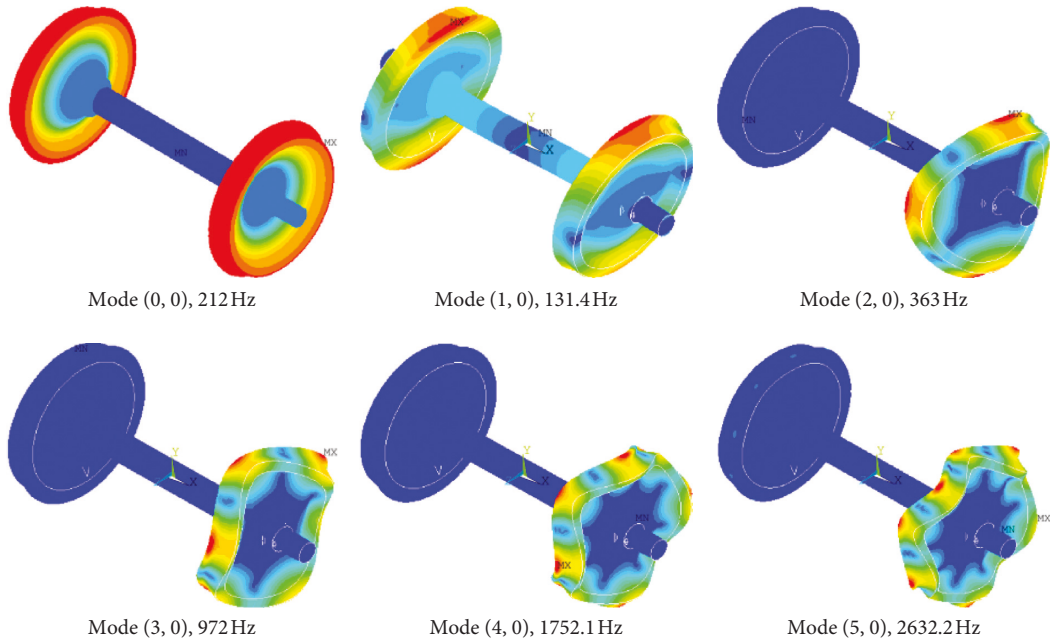

Figure 9: Wheel axial modes.

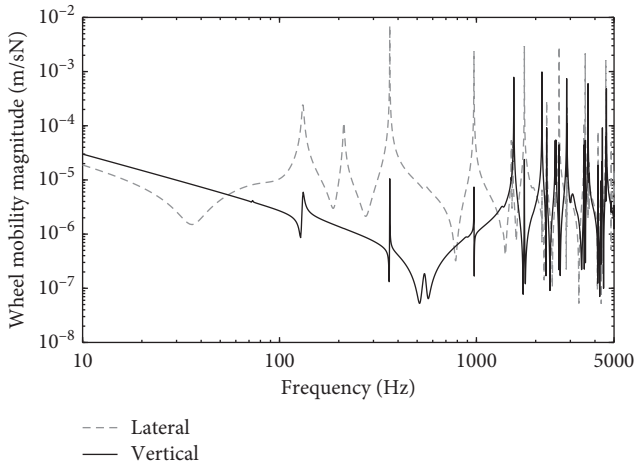

Figure 10: Wheel mobility.

which result in squeal. Figure 10 shows the lateral and vertical wheel mobility at the contact point. It can be seen that main peaks are around the axial mode frequencies.

The standard ballasted track model includes a UIC 60 rail and concrete sleepers with a sleeper spacing of 60 cm. Tables 3 and 4 summarize the railway track properties. The obtained lateral and vertical track mobility are illustrated in Figure 11.

Piezoelectric properties used in this study are presented in Table 5. It can be seen in Figure 9 that the wheel thread has maximum bending deformation in axial modes. In addition, the wheel thread surface (inside and outside) is flat. Therefore, they are satisfactory locations for attaching the piezoelectric patches. It is worth noticing the fact that the piezoelectric patches should not be placed on the node lines synchronously. Therefore, the number of the piezoelectric patches must be odd. Fifteen piezoelectric patches in every side of the wheel thread are attached. Patch dimensions

Table 3: UIC 60 rail properties [39].

Parameter	Symbol	Unit	Value
Elastic modulus	E	GPa	210
Density	ρ	kg/m^3	7850
Poisson's ratio	ν	—	0.3

Table 4: Track modeling parameters [39].

	C_b (kN·s/m)	K_b (MN/m)	M_s (kg)	C_{pr} (N·m·s)	K_{pr} (kN·m)	C_p (kN·s/m)	K_p (MN/m)
Lateral track model	48	80	162	163.5	654	12.5	50
Vertical track model	50	50	162	—	—	87.5	350

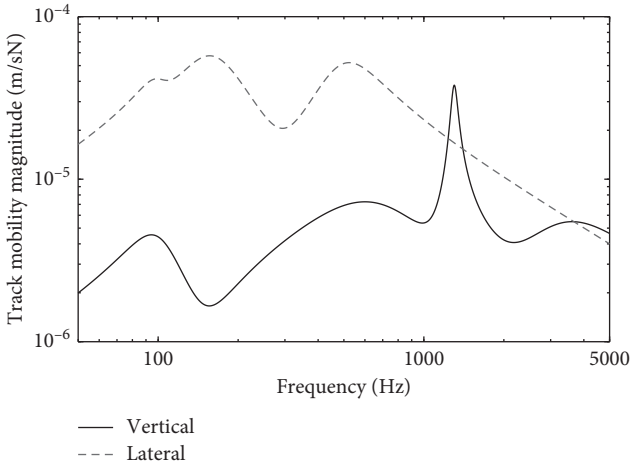

Figure 11: Track mobility.

Table 5: Piezoelectric properties [40].

Parameter	Symbol	Unit	Value
Relative permittivity	ε_{33}^T	—	1700
Piezoelectric constant	d_{31}	$\times 10^{-12}$ m/V	190
Compliance matrix	S_{33}^E	$\times 10^{-12}$ m^2/V	18.8
	S_{11}^E	$10e-12$ m^2/N$\times$	16.4
	S_{12}^E	$10e-12$ m^2/N$\times$	−5.74
	S_{13}^E	$10e-12$ m^2/N$\times$	−7.22
	S_{44}^E	$10e-12$ m^2/N$\times$	47.5
	S_{55}^E	$10e-12$ m^2/N$\times$	44.3
	S_{66}^E	$10e-12$ m^2/N$\times$	44.3

Table 6: Piezoelectric patch dimensions.

Parameter	Symbol		Value
Thickness	t_p		0.02 m
Length	L_p		0.163 m
Width	w_{pf}	Front	0.058 m
	w_{pb}	Back	0.04 m

(presented in Table 6) are chosen to be in allowable range presented by the manufacturer [37]. Additional patches do not essentially enhance the performance since their length should be reduced for this purpose and consequently short patches receive less stretch.

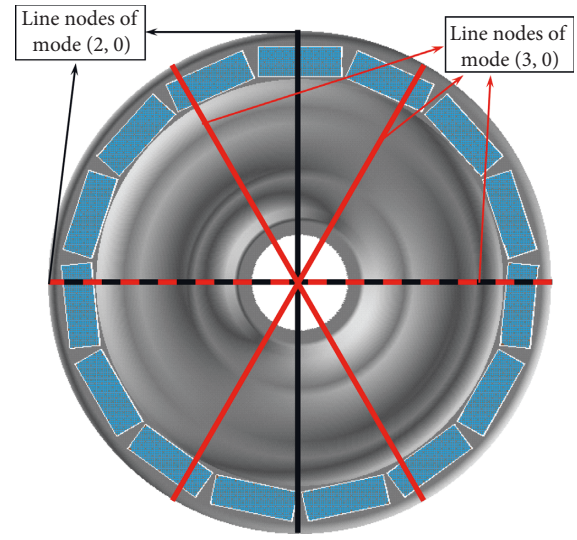

Figure 12: The piezoelectric patches layout on the wheel thread and node lines of mode (2, 0) and (3, 0).

As explained in Section 4.1, it is desired to add damping at the axial modes (2, 0) and (3, 0) as the main source of the squeal noise. The piezoelectric patches arrangement on the wheel thread is shown in Figure 12. Also node lines of mode (2, 0) and (3, 0) are drawn in accordance with Figure 9. It is seen that if the number of piezoelectric patches is odd (assumed to be 15 in this figure), we can have maximum number of patches allocated on $k\pi/2$ and $k\pi/3$ ($k = 1, 4$) lines of action. For instance if we add an extra patch and increase the number of patches from 15 to 16 in this figure, we loose 4 of the effective patches in lines of $k\pi/3$ and we gain only one extra patch at line $3\pi/2$.

4. Results

In this section, numerical results of the wheel squeal simulation are presented for different conditions. Wheel squeal modeling with no added damping is presented, and the most effective mode shapes are identified. The primary analysis is utilized to design optimal shunt circuit. Subsequently, simulation results for different damped wheels with miscellaneous shunt circuits and layouts are analyzed and compared.

4.1. Wheel Squeal Simulation. Determining the dominant unstable modes that have main effect on wheel squeal occurrence is necessary for the shunt circuit design. For this

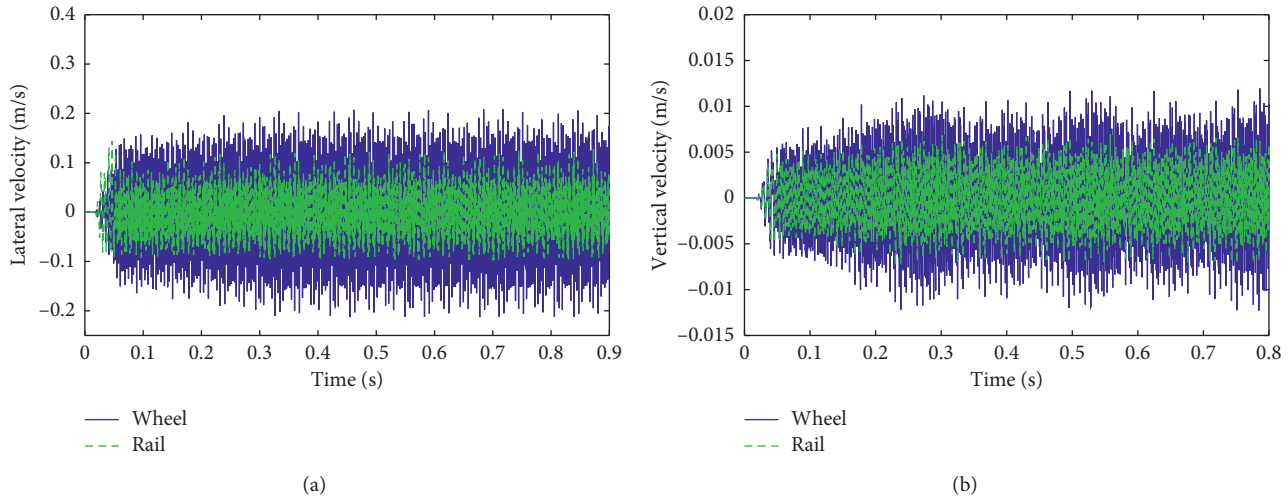

Figure 13: Time history of the (a) lateral velocity and (b) vertical velocity.

purpose, the wheel squeal with no extra damping simulation results is illustratively analyzed. The time history of lateral and vertical velocities of the rail and wheel are shown in Figures 13(a) and 13(b). It can be seen that the wheel lateral velocity is much higher than the rail. Moreover, the wheel has a wider vibrating area. Since the emitted noise corresponds to (area) × (velocity) according equation (13), it can be expected that the wheel acts as the main source. Furthermore, lateral velocity is 20 times larger than the vertical velocity. This allows one to only take lateral wheel vibration into account for calculations.

The FFT (fast Fourier transform) algorithm is used for calculating frequency response from time history. Frequency spectrum of the wheel lateral velocity is illustrated in Figure 14(a). It is observed that the axial modes, particularly modes (2, 0), (3, 0), and (0, 0), are the main unstable modes and sources of the squeal noise. This claim is proven in Figure 14(b). This figure shows the sound pressure level (SPL) at a point 1.0 meter away from the wheel is calculated by the method presented in Section 2.5 in the third octave-band spectrum. It is seen that the maximum SPL is 113 dB and 108 dB around the modes (3, 0) and (2, 0), respectively. Higher sensitivity of the human ears to high frequencies influences the problem so that the shunted piezoelectric must provide utmost damping in such modes.

Figure 15 shows the SPL through a 0.5 m × 0.5 m surface and 0.1 meter and 2.5 meter away from the wheel. It can be observed in Figures 15(a) and 15(c) that the highest SPL is around the wheel thread where axial modes have maximum deformation.

4.2. Wheel Squeal Simulation with Damped Wheel. In this section, performance of the shunted piezoelectric system in mitigating the wheel squeal noise is studied. Two shunt circuits, i.e., *R* and *RL*, are considered. Piezoelectric properties are optimally found by the method presented in Section 2.6.1 and listed in Table 7.

Four different scenarios are proposed and compared. In the first scenario, every two patches in both sides of the wheel thread are connected to a *RL* shunt circuit and adjusted to the mode (2, 0). It means that all the couple patches are planned to add damping in a single mode. The second scenario is similar to the first one; however, it aims at to add damping in the mode (3, 0). Results of these two scenarios are compared in Figure 16(a) (SPL in octave-band), Figure 16(b) (lateral wheel velocity), and Figure 17 (frequency spectrum of lateral wheel velocity). As seen, the applied strategy reduces the SPL and the wheel response around the adjusting frequency but is not effective on other frequencies. It is seen that even the SPL and lateral wheel velocity are boosted in mode $(n, 0)$ with $n \geq 3$. It shows that the mode $(n, 0)$ with $n \geq 3$ is coupled with mode (3, 0). It means that if the mode (3, 0) becomes unstable other modes also get unstable and the wheel lateral velocity fluctuates in higher frequencies. The modes (0, 0) and (1, 0) are coupled to the mode (2, 0) and behave similarly. It can be observed from Figure 17 that the peak on the mode (2, 0) completely disappeared but extra peaks appeared in frequencies higher than the mode (3, 0). The similar behavior can be seen between the modes (2, 0) and (1, 0). According to these results, we can conclude that the SPL and the wheel vibration cannot be reduced effectively by adding damping in a single mode. Also the corresponding added damping in different frequencies is calculated by the method presented in Section 2.6.1 for each scenario and listed in Table 8.

The third scenario is similar to the first one but the resonant circuit is replaced by the resistive circuit with similar adjusting frequency i.e., (2, 0). The circuit provides lower damping in the mode (2, 0), but it acts more effectively in other frequencies. It can be seen in Figures 16 and 17 that although the SPL and the wheel vibration are not very much suppressed around the mode (2, 0), the circuit performance enhances in higher frequencies. A reduction of 25 dB in the SPL is achieved around the mode (3, 0).

The fourth scenario is aimed at providing optimal damping simultaneously for both modes (2, 0) and (3, 0). The layout is the same as the first approach with *RL* elements,

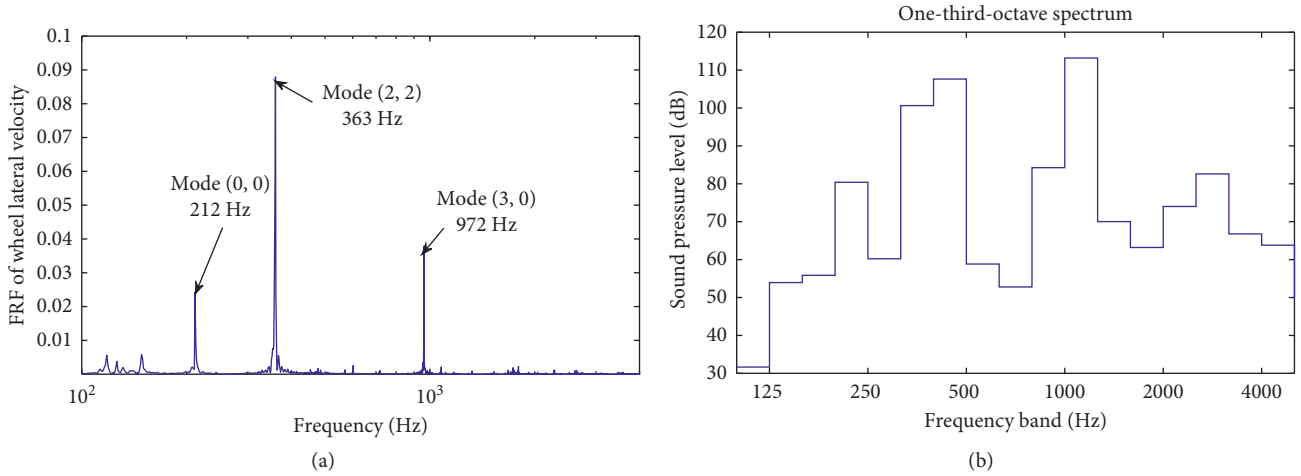

FIGURE 14: (a) FRF of wheel lateral velocity. (b) Sound pressure level on $X = 1$ m.

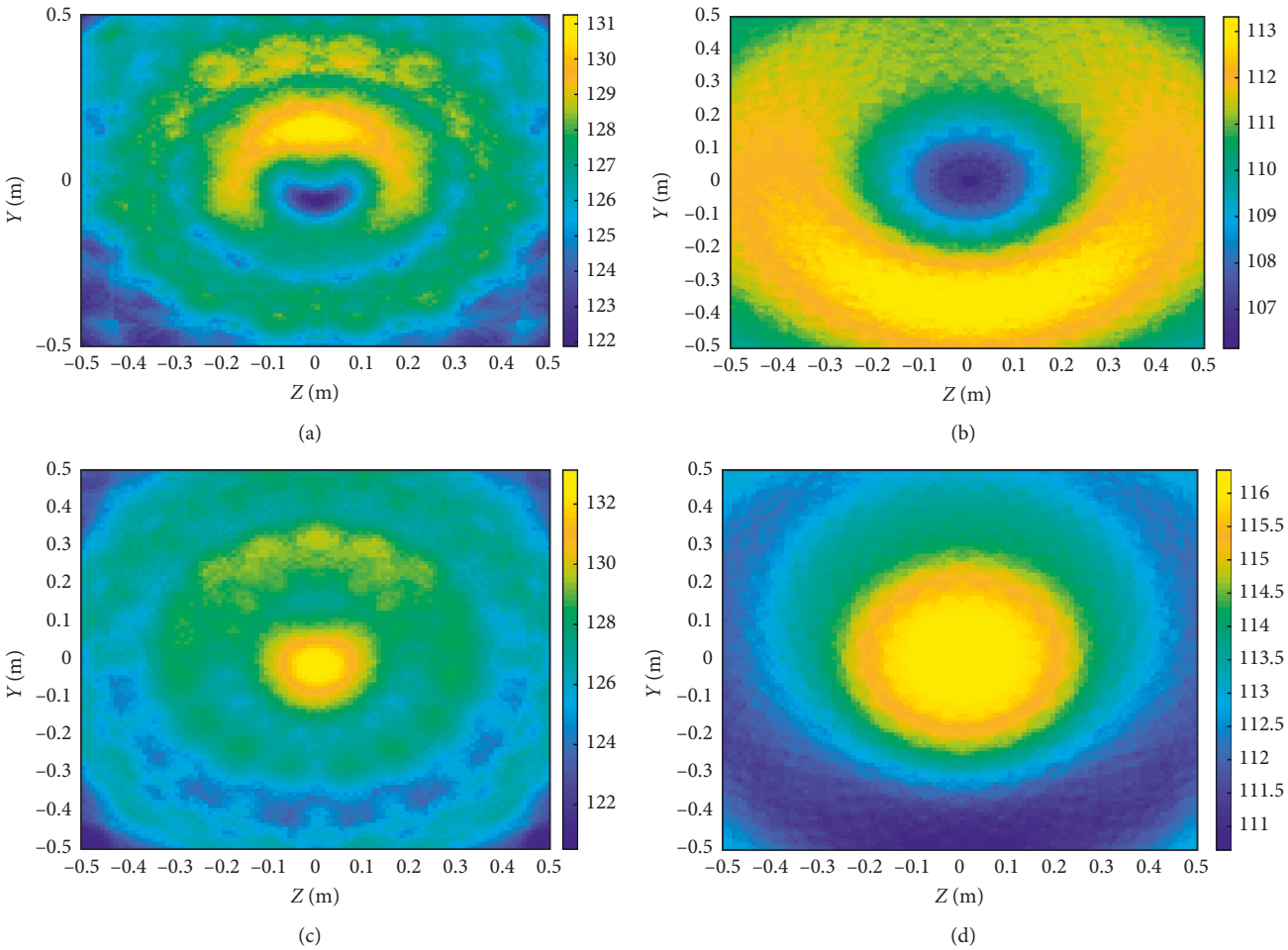

FIGURE 15: Sound pressure level variation through position and time. (a) $X = 0.1$ m, $t = 0.75$ s. (b) $X = 2.5$ m, $t = 0.75$ s. (c) $X = 0.1$ m, $t = 0.7504$ s. (d) $X = 2.5$ m, $t = 0.7504$ s.

but the shunt circuits are divided into two groups. The first group (eight patches) is adjusted to the mode (2, 0), and the rest of them are tuned to the mode (3, 0).

Figures 18 and 19 indicate that both the SPL and the wheel lateral velocity are effectively mitigated at all frequencies. 9.0 dB reduction in the SPL around the mode (2, 0) and 46.0 dB around the mode (3, 0) are simultaneously achieved. Based on the results shown in Figure 19, one can conclude that the mode (3, 0) and higher modes are significantly suppressed.

Table 7: Optimum parameters of the shunt circuits.

Shunt circuit	R	RL	RL
Frequency	Mode (2, 0), 363 Hz	Mode (2, 0), 363 Hz	Mode (3, 0), 972 Hz
R (Ω)	25,000	2100	600
L (H)	—	11.2	1.56

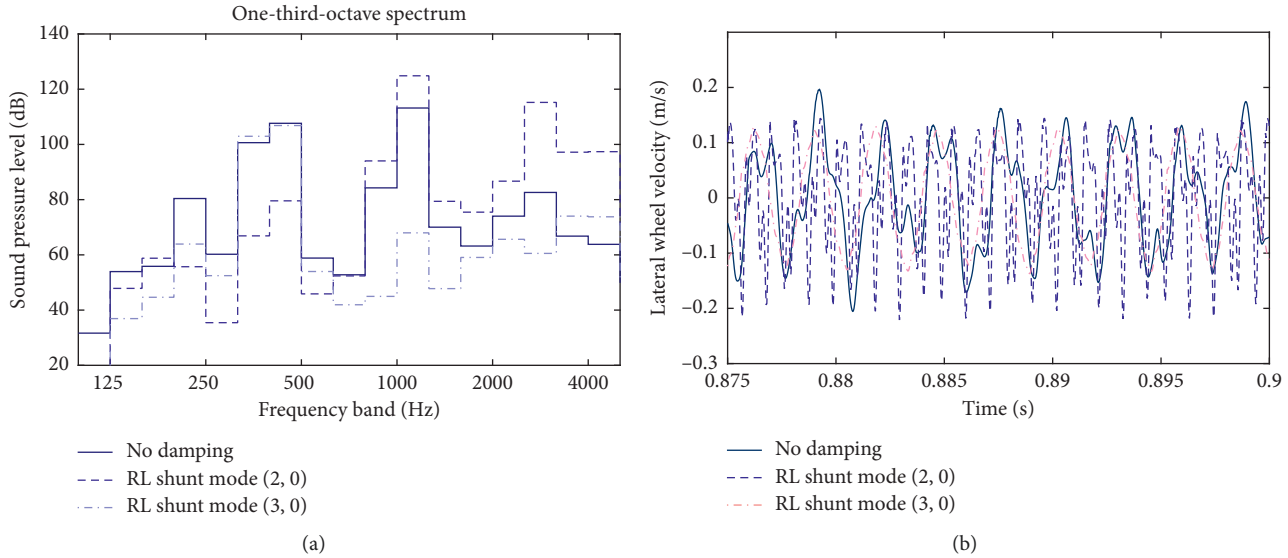

Figure 16: (a) Performance of the RL shunt circuit in decreasing the SPL $X = 1$ m. (b) Performance of the RL shunt circuit in decreasing the wheel vibration (time domain).

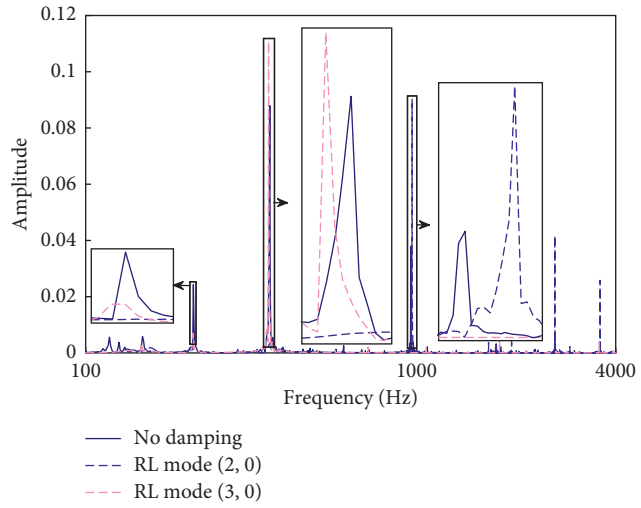

Figure 17: Performance of the RL shunt circuit in decreasing the wheel vibration (frequency domain).

Table 8: Added damping in different cases.

	Shunt circle	Damping in mode (2, 0), 363 Hz	Damping in mode (3, 0), 972 Hz
Case 1	RL	0.037	$4.00E-05$
Case 2	RL	$4.00E-05$	0.04
Case 3	R	$9.89E-04$	$7.76E-04$
Case 4	RL	0.0227	0.0332

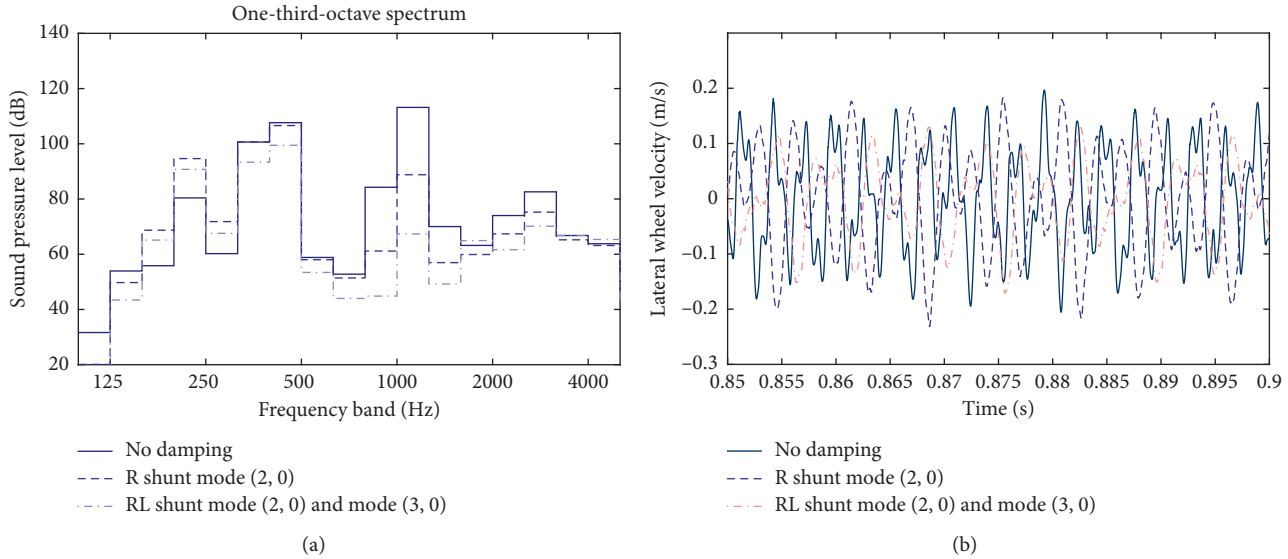

Figure 18: (a) Performance of the R and multimode RL shunt circuits in decreasing the SPL $X = 1$ m. (b) Performance of the R and multimode RL shunt circuits in decreasing the wheel vibration (time domain).

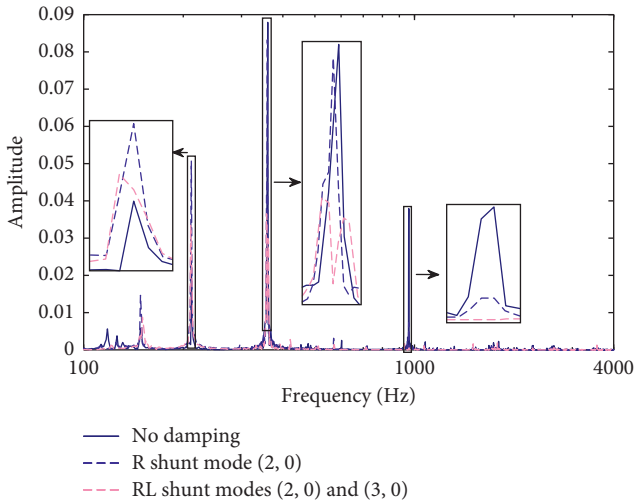

Figure 19: Performance of the R and multimode RL shunt circuits in decreasing the wheel vibration (frequency domain).

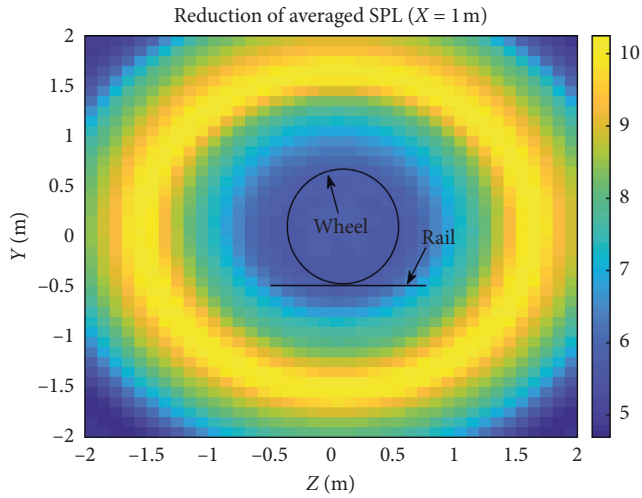

Figure 20: Performance of the multimode RL shunt circuits in decreasing the wheel squeal in the SPL.

Figure 20 illustrates the sound pressure level reduction around the wheel in near-field and far-field. In order to achieve the shown results, the pressure field has been calculated and compared for the wheel with and without passive control system. A remarkable noise reduction in the near-field (up to 5 dB) and the far-field (up to 10 dB) is achieved.

5. Conclusion

A new methodology for mitigation of squealing noise in railway applications was proposed. Application of piezoelectric elements in wheel noise reduction was evaluated in the time domain. A comprehensive model including the wheel and track and their interaction was employed. Vibration of the wheel surface was obtained when it runs over a sharp curved track. The consequent sound pressure level of the wheel noise was found by employing the Rayleigh integral. Two different configurations of the piezoelectric elements were applied to the head section of the wheel. Performance of different shunt circuits including the R and RL was investigated in different frequency ranges. It was found that for the RL shunt circuit tuned to the mode (2, 0), and all the higher modes $(n, 0)$ with $n \geq 3$ became unstable. If it is tuned to the mode (3, 0), it would perform well on the higher modes but has no remarkable effect on the mode (2, 0). Changing to the R shunt circuit, one can achieve the damping not only for the tuned mode, but also for higher and lower modes. However, there is still deficiency regarding the small and inadequate value of added damping.

Multimode damping was achieved by dividing piezoelectric patches into two different clusters, one acting on the

mode (2, 0) and the other on (3, 0). According to the obtained results, vibration of the wheel surface as well as the SPL of the wheel squeal noise can remarkably be reduced by such a multimode reductive system. The proposed system can provide damping more than 2% in axial modes, which is significantly higher than the damping provided by other methods. Another advantage is predictability of the dynamic behavior of the system which is an important issue in such types of control systems.

Data Availability

Numerical data are available upon request from the corresponding author.

Conflicts of Interest

The authors declare that they have no conflicts of interest.

References

[1] J. Oertli, *Combating Curve Squeal Phase II—Final Report*, Union Internationale des Chemins de fer Swiss Federal Railways (SBB), Paris, France, 2005.

[2] R. Grubliauskas, B. Strukcinskiene, J. Raistenskis et al., "Relation between the railroad noise and the social-economic factors," *Journal of Vibroengineering*, vol. 16, no. 2, pp. 987–996, 2014.

[3] M. A. Heckl and I. D. Abrahams, "Curve squeal of train wheels, part 1: mathematical model for its generation," *Journal of Sound and Vibration*, vol. 229, no. 3, pp. 669–693, 2000.

[4] I. Merideno, J. Nieto, N. Gil-Negrete, A. Landaberea, and J. Iartza, "Constrained layer damper modelling and performance evaluation for eliminating squeal noise in trams," *Shock and Vibration*, vol. 2014, Article ID 473720, 11 pages, 2014.

[5] H. Tetsuya, T. Yano, and Y. Murakami, "Annoyance due to railway noise before and after the opening of the Kyushu Shinkansen Line," *Applied Acoustics*, vol. 115, pp. 173–180, 2017.

[6] R. Stefanelli, J. Dual, and E. Cataldi-Spinola, "Acoustic modelling of railway wheels and acoustic measurements to determine involved eigenmodes in the curve squealing phenomenon," *Vehicle System Dynamics*, vol. 44, no. sup 1, pp. 286–295, 2006.

[7] N. Vincent, J. R. Koch, H. Chollet, and J. Y. Guerder, "Curve squeal of urban rolling stock-part 1: state of the art and field measurements," *Journal of Sound and Vibration*, vol. 293, no. 3–5, pp. 691–700, 2006.

[8] M. A. Pallas, J. Lelong, and R. Chatagnon, "Tram noise emission: spectral analysis of the noise source contributions," *The Journal of the Acoustical Society of America*, vol. 123, no. 5, p. 3384, 2008.

[9] J. R. Koch, N. Vincent, H. Chollet, and O. Chiello, "Curve squeal of urban rolling stock-Part 2: parametric study on a 1/4 scale test rig," *Journal of Sound and Vibration*, vol. 293, no. 3–5, pp. 701–709, 2006.

[10] P. A. Meehan, P. Bellette, X. Liu, C. Milne, and D. Anderson, "Investigation of wheel squeal characteristics using a rolling contact two disk test rig," in *Proceedings of the 9th World Conference on Railway Research*, Lille, France, May 2011.

[11] Z. Huang, D. J. Thompson, and C. Jones, "Squeal prediction for a bogied vehicle in a curve," in *Proceedings of the Noise and Vibration Mitigation for Rail Transportation Systems*, pp. 313–319, Springer, Munich, Germany, September 2008.

[12] X. Liu, P. Bellette, C. Milne, and P. Meehan, "Investigation about the effect of angle of attack and relative humidity on wheel squeal," in *Proceedings of Acoustics*, Gold Coast, Australia, November 2011.

[13] D. J. Thompson and A. D. A. Monk-Steel, "Theoretical model for curve squeal," Technical report, University of Southampton, Institute of Sound and Vibration Research, Southampton, UK, 2003.

[14] C. Glocker, E. Cataldi-Spinola, and R. I. Leine, "Curve squealing of trains: measurement, modelling and simulation," *Journal of Sound and Vibration*, vol. 324, no. 1-2, pp. 365–386, 2009.

[15] X. Liu and P. Meehan, "The modeling of wheel squeal in the time domain and its validation," in *Proceedings of Meetings on Acoustics*, Montreal, Canada, June 2013.

[16] J. Jiang, D. Anderson, and R. Dwight, "The mechanisms of curve squeal," in *Proceedings of the Noise and Vibration Mitigation for Rail Transportation Systems*, pp. 587–594, Springer, 2015.

[17] X. Liu and P. A. Meehan, "Wheel squeal noise: a simplified model to simulate the effect of rolling speed and angle of attack," *Journal of Sound and Vibration*, vol. 338, pp. 184–198, 2015.

[18] I. Zenzerovic, A. Pieringer, and W. Kropp, "Towards an engineering model for curve squeal," in *Proceedings of the Noise and Vibration Mitigation for Rail Transportation Systems*, pp. 433–440, Springer, Uddevalla, Sweden, September 2013.

[19] D. Younesian, M. H. Aleghafourian, and E. Esmailzadeh, "Vibration analysis of circular annular plates subjected to peripheral rotating transverse loads," *Journal of Vibration and Control*, vol. 21, no. 7, pp. 1443–1455, 2015.

[20] B. Müller and J. Oertli, "Combating curve squeal: monitoring existing applications," *Journal of Sound and Vibration*, vol. 293, no. 3–5, pp. 728–734, 2006.

[21] D. Curley, D. Anderson, J. Jiang, and D. Hanson, "Field trials of gauge face lubrication and top-of-rail friction modification for curve noise mitigation," in *Noise and Vibration Mitigation for Rail Transportation Systems*, pp. 449–456, Springer, Berlin, Germany, 2015.

[22] D. Hanson, J. Jiang, B. Dowdell, and R. Dwight, "Curve squeal: causes, treatments and results," in *Proceedings of the INTER-NOISE and NOISE-CON Congress and Conference*, pp. 6316–6323, Melbourne, Australia, November 2014.

[23] N. Garg and O. Sharma, "Noise emissions of transit trains at curvature due to track lubrication," *Indian Journal of Pure & Applied Physics*, vol. 48, pp. 881–885, 2010.

[24] E. J. M. Hiensch and J. W. Lammers, "Preventing railway squeal noise through railhead optimisation," in *Proceedings of the 8th Congress on the Railway Research*, pp. 18–22, Seoul, South Korea, May 2008.

[25] J. F. Brunel, P. Dufrénoy, J. Charley, and F. Demilly, "Analysis of the attenuation of railway squeal noise by preloaded rings inserted in wheels," *The Journal of the Acoustical Society of America*, vol. 127, no. 3, pp. 1300–1306, 2010.

[26] D. H. Koo, J. C. Kim, W. H. Yoo, and T. W. Park, "An experimental study of the effect of low-noise wheels in reducing noise and vibration," *Transportation Research Part D: Transport and Environment*, vol. 7, no. 6, pp. 429–439, 2002.

[27] R. Fan, G. Meng, J. Yang, and C. He, "Internal noise reduction in railway carriages: a case study in China," *Transportation*

Research Part D: Transport and Environment, vol. 13, no. 4, pp. 213–220, 2008.

[28] R. Shakeri and D. Younesian, "Broad-band noise mitigation in vibrating annular plates by dynamic absorbers," *International Journal of Structural Stability and Dynamics*, vol. 116, no. 6, Article ID 550014, 2015.

[29] S. R. Moheimani and A. J. Fleming, *Piezoelectric Transducers for Vibration Control and Damping*, Springer Science & Business Media, Berlin, Germany, 2006.

[30] T. P. Sales, D. A. Rade, and L. C. G. De Souza, "Passive vibration control of flexible spacecraft using shunted piezoelectric transducers," *Aerospace Science and Technology*, vol. 29, no. 1, pp. 403–412, 2013.

[31] J. D. Tippmann and F. L. di Scalea, "Vibration control experiments using piezoelectric transducers on a wind turbine blade," in *Proceedings of the SPIE Smart Structures and Materials+ Nondestructive Evaluation and Health Monitoring*, Pueblo, CO, USA, April 2013.

[32] T. Takigami and T. Tomioka, "Bending vibration suppression of railway vehicle carbody with piezoelectric elements," *Journal of Mechanical Systems for Transportation and Logistics*, vol. 1, no. 1, pp. 111–121, 2008.

[33] A. Jakob, M. Stuz, J. Feldmann, and M. Moser, "Experiments on active vibration control of a scale model rail wheel," in *Proceedings of Euro Noise*, Tampere, Finland, May 2006.

[34] S. R. Marjani and D. Younesian, "Suppression of the train wheel squeal noise by shunted piezoelectric elements," *International Journal of Structural Stability and Dynamics*, vol. 17, no. 2, Article ID 1750027, 2017.

[35] C. J. C. Jones and D. J. Thompson, "Rolling noise generated by railway wheels with visco-elastic layers," *Journal of Sound and Vibration*, vol. 231, no. 3, pp. 779–790, 2000.

[36] T. X. Wu and D. J. Thompson, "Analysis of lateral vibration behavior of railway track at high frequencies using a continuously supported multiple beam model," *The Journal of the Acoustical Society of America*, vol. 106, no. 3, pp. 1369–1376, 1999.

[37] J. J. Kalker, "Wheel-rail rolling contact theory," *Wear*, vol. 144, no. 1-2, pp. 243–261, 1991.

[38] N. W. Hagood and A. Von Flotow, "Damping of structural vibrations with piezoelectric materials and passive electrical networks," *Journal of Sound and Vibration*, vol. 146, no. 2, pp. 243–268, 1991.

[39] N. Vincent and D. J. Thompson, "Track dynamic behaviour at high frequencies. Part 2: experimental results and comparisons with theory," *Vehicle System Dynamics*, vol. 24, no. sup1, pp. 100–114, 1995.

[40] Midé, *QuickPack Products: Material Properties & Spec Sheets*, Midé Technology Corporation, Medford, MA, USA, 2014.